PROCEEDINGS, 48th Workshop on Geothermal Reservoir Engineering
Stanford University, Stanford, California, February 6-8, 2023
SGP-TR-224

Thermodynamics and Economics Analysis of Utilization of Ionic Liquids in Kalina Cycle System 34

Deny Fajar Riansyah*, Tubagus Ahmad Fauzi Soelaiman, Firman Bagja Juangsa, and Azaria Haykal Ahmad

Faculty of Mechanical and Aerospace Engineering, Institut Teknologi Bandung, Bandung, Indonesia

E-mail: denyriansyah.dr@gmail.com

Keywords: geothermal bottoming unit, absorption power cycle, Kalina Cycle, ionic liquids

ABSTRACT

The awareness of the effect of climate change due to the extensive burning fossil fuels has been increasing recently. Reducing the use of fossil fuels can be done by increasing the efficiency of fossil power plants and/or by using renewable energy resources. Geothermal, as one of the renewable energy resources, has been developed in power plants by utilizing its unused brine for bottoming cycle. This study focuses on using Kalina cycle system (KCS) 34 with ionic liquids of water-[EMIM][DMP] as the working fluid to generate electricity from unused brine in a geothermal power plant. The modeling of thermodynamic properties of the ionic liquids and using KCS 34 has been carried out using the MATLAB R2020b software. Thermodynamics analysis was conducted to find the optimum condition to produce maximum net power and thermal efficiency. Then, an economics analysis was performed by calculating the estimated capital cost and the payback period as well as the gross income at its optimum point. In addition, the analysis was also carried out by comparing the performance with ammonia-water. The results of the optimization using water-[EMIM][DMP] gives maximum net power and thermal efficiency of 343.23 kW and 8.81%, respectively, which is about 5.18% higher than if using ammonia-water. The estimated capital cost is $2,753,426.94, or about 3.77% higher; with a gross income of $319,055.66/year, or about 5.38% higher. The use of water-[EMIM][DMP] requires a payback period of 9 years since the system starts operating, or about a month earlier than if using ammonia-water.

1. INTRODUCTION

With the growing demand for electrical energy, the Indonesian government needs to increase the national power generation capacity. Based on the Electricity Supply Business Plan (RUPTL) of the National Electricity Company (PLN) 2021—2038, the average growth in Indonesia's electricity demand can reach 4.9% per year (Direktorat Jenderal Ketenagalistrikan, 2021). The use of new and renewable energy (NRE) based power plants is still relatively low compared to fossil energy. The government targets using NRE-based power plants for at least 23% of the total energy mix by 2025 (Rencana Umum Energi Nasional, 2017).

The utilization of renewable energy resources is still 8.8% in Indonesia, so Indonesia has an opportunity to develop NRE-based power plants by utilizing geothermal energy. Until 2019, the utilization of high-temperature geothermal reservoirs has reached 80%. Therefore, the use of geothermal reservoirs at moderate temperatures is needed to reach the national energy mix target in 2025. The technology that can be used to utilize medium-temperature geothermal energy is using a binary cycle, such as the Organic Rankine Cycle (ORC), and a Kalina Cycle (Badan Geologi, 2018).

The Kalina Cycle uses an ammonia-water fluid. In terms of sustainability, ammonia is toxic and flammable (Bacharach, 2020). The toxic nature of ammonia in the Kalina Cycle gives potential hazards. Therefore, further studies and research on safer alternative working fluids are needed to overcome these hazards. A new working fluid mixture of ionic liquids has non-toxic properties, low risk of corrosiveness, and no potential for crystallization to occur has been discovered (Khamooshi et al., 2013). Simulation of thermodynamic performance in the Absorption Refrigeration Cycle using a mixture of ionic liquids, namely water with *1-ethyl-3-methylimidazolium dimethyl phosphate* ([EMIM][DMP]) compared to *lithium bromide* solution gives *coefficient of performance* (COP) of 7% lower, but still above 0.7 (Zhang & Hu, 2011). The ionic liquids mixture can be considered an alternative working fluid in the Kalina Cycle.

2. DESCRIPTION OF THE STUDY SITE

To study the use of the ionic liquid mixture in a geothermal power plant, the Lahendong geothermal power plant has been chosen as the case study as it produces large amount of brine. The plant is located in Tomohon, North Sulawesi, Indonesia as shown in Figure 1. Specifications of the brine produced that will be used as the heat source in the Lahendong can be seen in **Error! Reference source not found.**.

Figure 1: Location of Lahendong Geothermal Field (earth.google.com, 2020).

Table 1: Specifications of brine in Lahendong Geothermal Power Plant (Frick et al., 2015).

Parameter	Value	Unit
The temperature of the brine leaving the separator	170	°C
Minimum brine temperature entering the injection well	140	°C
Brine mass flow	110	ton/h

3. DESCRIPTION OF THE CYCLE

The Kalina cycle is a thermodynamic cycle invented by a Russian scientist, Dr. Alexander Kalina, in the 1980s (Zhang et al., 2012). The Kalina cycle uses a mixed working fluid consisting of two fluids. Until 2021, the variations of Kalina cycle have been categorized into two generations. Compared to the first generation, the second-generation of Kalina Cycles is claimed to have higher thermal efficiency but at higher capital costs (Ahmad & Karimi, 2016). The Kalina Cycle is special since the evaporation and condensation processes in the cycle occur at non-constant temperatures due to the nature of the mixed fluid. This phenomenon allows the cycle to work more efficiently than the constant temperature process, and the cycle can be adaptive to changes of the temperature of the geothermal sources (Kalina et al., 2014). Dr. Alexander Kalina claims that the Kalina Cycle can provide up to 24% higher of thermal efficiency than ORC (Kalina et al., 2014).

One of the first generation Kalina Cycle systems often applied to geothermal energy power plants is KCS 34. According to Dr. Alexander Kalina, KCS 34 operates optimally at low temperatures (below 148°C). However, when operating above that temperature, the power generated is approximately the same as the ORC (Kalina et al., 2014). The schematic diagram of KCS 34 cycle can be seen in **Figure 2**.

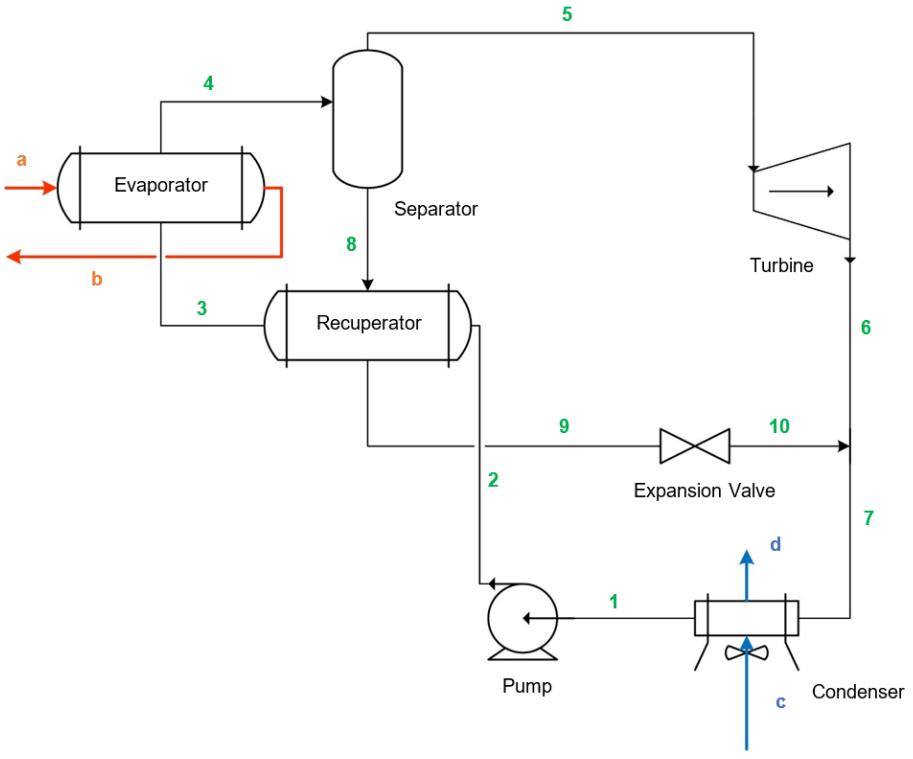

Figure 2: Process flow diagram of KCS 34.

4. MODELING AND SIMULATION

4.1. General

The selection of ionic liquids [EMIM][DMP] is based on the best thermodynamic performance among other ionic liquids in simulations in the Absorption Refrigeration Cycle (Zhang & Hu, 2011). In this study, an analysis of the performance of the Kalina Cycle System 34 was carried out with the working fluid in the form of a mixture of ionic liquids, namely water-[EMIM][DMP], and compare it's performace if using ammonia solution. Analysis of the performance of the Kalina Cycle 34 with the working fluid of an ionic liquid mixture was carried out with the help of the MATLAB R2020b software. After obtaining the optimum operating point, the research was carried out by calculating the estimated capital cost needed to develop the cycle and the payback period. The mass and energy balances of KCS 34 can be seen in

Table 2.

Table 2: Mass and energy balances of KCS 34.

Component	Mass balance	Energy balance
Pump Type: centrifugal pump	$\dot{m}_1 = \dot{m}_2 = \dot{m}$	$\dot{W}_{po} = \dot{m}(h_2 - h_1)$
Recuperator Type: shell & tube with counterflow	$\dot{m}_2 = \dot{m}_3$, $\dot{m}_8 = \dot{m}_9 = (1-u).\dot{m}$	$(h_3 - h_2) = (1-u)(h_8 - h_9)$
Evaporator Type: shell & tube with counterflow	$\dot{m}_3 = \dot{m}_4$, $\dot{m}_a = \dot{m}_b = \dot{m}_{gf}$	$\dot{Q}_{ev} = \dot{m}_{gf}(h_a - h_b) = \dot{m}(h_4 - h_3)$
Separator Type: vertical	$\dot{m}_4 = \dot{m}_8 + \dot{m}_5$	$h_4 = (1-u)h_8 + uh_5$
Turbine Type: axial turbine	$\dot{m}_5 = \dot{m}_6 = u.\dot{m}$	$\dot{W}_{tu} = \dot{m}(h_5 - h_6)$
Expansion valve Type: globe valve	$\dot{m}_9 = \dot{m}_{10}$	$h_9 = h_{10}$
Mixer	$\dot{m}_7 = \dot{m}_6 + \dot{m}_{10}$	$h_7 = uh_6 + (1-u)h_{10}$
Condenser Type: air-cooled condenser	$\dot{m}_7 = \dot{m}_1$, $\dot{m}_c = \dot{m}_d = \dot{m}_{cf}$	$\dot{Q}_{cond} = \dot{m}_{cf}(h_d - h_c) = \dot{m}(h_7 - h_1)$

This study used thermodynamic and economic assumptions in conducting simulations and calculations. The thermodynamic assumptions used are as follow:

- Geothermal fluid is pure water (Novotny & Kolovratnik, 2016).
- The system of each component is analyzed at a steady-state (Moran et al., 2014).
- Changes in potential and kinetic energies in each system are neglected (Moran et al., 2014).
- The condenser uses air cooling fluid with input and output temperatures of 25°C and 40°C, respectively (D. Mendrinos et al., 2020).
- The isentropic efficiency of the turbine and pump is 85% (Franco & Villani, 2009).
- No pressure drop in piping systems, heat exchanger components, and separators (Li et al., 2013).
- No heat transfer between components and environment (Li et al., 2013).
- The mass flow rate of the working fluid is 5 kg/s (Kumara et al., 2015).
- Condensing pressure is 0.1 bar (Ranjan et al., 2013).
- Preheater exit fluid condition is limited to the saturated liquid phase (Franco & Villani, 2009).
- The condition of the fluid entering the pump is saturated liquid (Franco & Villani, 2009).
- The *pinch point temperature difference* (PPTD) on the heat exchanger component is 10°C (DiPippo, 2005).

The economic assumptions used are as follow:

- Calculation of the cost of capital for the two KCS 34 systems is an estimated cost and there are still factors that are not taken into account in this analysis (Putera et al., 2019).
- The selling price of electricity, operating and maintenance costs, capacity factor, and bank loan interest rates from these two systems are considered constant each year (Putera et al., 2019).
- In both systems, a turn-around activity is carried out once every five years with a duration of thirty days (Energia News, 2021).
- The CEPCI (Chemical Engineering Plant Cost Index) factor used is the latest value in 2021 (Putera et al., 2019).

4.2. Vapor-liquid equilibrium (VLE)

The vapor-liquid equilibrium modeling of ammonia-water fluid was carried out by utilizing the numerical equations for the parameters of the bubble temperature and dew temperature, which depend on the composition and the pressure of the constituent fluid. J. Patek and J. Klomfar have modeled numerically (Pátek & Klomfar, 1995), which has been validated at a pressure of 0.2—20 bar, as shown in Equations (1) and (2), and the coefficients and constants can be seen in **Table A.1**,

$$T_{bbl}(p,x) = 100\sum_i b_i(1-x)^{m_i}\left[\ln\left(\frac{2}{p}\right)\right]^{n_i} \quad (1)$$

$$T_{dew}(p,x) = 100\sum_i b_i(1-y)^{\frac{m_i}{4}}\left[\ln\left(\frac{2}{p}\right)\right]^{n_i} \quad (2)$$

Modeling of vapor-liquid equilibrium in water-[EMIM][DMP] fluid is using Modified Raoult's Law. The saturated vapor pressure is calculated using the Antoine equation. Fluids are assumed to be non-ideal solutions under liquid conditions and ideal gasses under vapor conditions. The activity coefficient was calculated using the NRTL (Non-Random-Two-Liquid) method. The Antoine equation can be seen in Equation (3) as follows (Smith et al., 2018),

$$\ln(100p^{sat}) = b_1 + \frac{b_2}{(b_3 + T + 273.15)} \quad (3)$$

Modeling the saturated vapor pressure of water using Equation (3) and constants can be seen in **Table A.2**. This equation is valid for use at a temperature of 0—200°C (Ren et al., 2011). Since [EMIM][DMP] is a non-volatile fluid, the value of the saturated vapor pressure can be neglected. The NRTL equations can be seen in Equations (4) and (5) using the coefficients in **Tables A.3** and **A.4**,

$$\ln\gamma_1 = x_2^2\left[\tau_{21}\left(\frac{G_{21}}{x_1 + x_2G_{21}}\right)^2 + \frac{G_{12}\tau_{12}}{(x_2 + x_1G_{12})^2}\right] \quad (4)$$

$$\ln\gamma_2 = x_1^2\left[\tau_{12}\left(\frac{G_{12}}{x_2 + x_1G_{12}}\right)^2 + \frac{G_{21}\tau_{21}}{(x_1 + x_2G_{21})^2}\right] \quad (5)$$

with,

$$G_{12} = \exp(-\alpha\tau_{12}) \qquad G_{21} = \exp(-\alpha\tau_{21})$$
$$\tau_{12} = \frac{b_{12}}{RT} \qquad \tau_{21} = \frac{b_{21}}{RT}$$
$$b_{12} = a_1 + b_1T + c_1T^2 \qquad b_{21} = a_2 + b_2T + c_2T^2$$

4.3. Enthalpy and entropy of fluids

The enthalpy and entropy modelings in the ammonia-water fluid used the enthalpy and entropy parameters of the pure fluid by adding excess enthalpy parameters. B. Ziegler and C. Trepp modeled a simple numerical equation for the enthalpy and entropy of pure ammonia and water that is valid for temperature of 230—500 K and pressure of 0.2—50 bar (Ziegler & Trepp, 1984) as can be seen in Equations (6) , (7) , (9) and (10).

$$h_{fl} = -100.R\left\{-b_{fl,1} + b_{fl,2}\left[b_{fl,3} - \frac{T}{100}\right] + \frac{b_{fl,4}}{2}\left[{b_{fl,3}}^2 - \left(\frac{T}{100}\right)^2\right] + \frac{b_{fl,5}}{3}\left[{b_{fl,3}}^3 - \left(\frac{T}{100}\right)^3\right] + \left[b_{fl,6}\left(\frac{T}{100}\right)^2 - b_{fl,7}\right]\left[\left(\frac{p}{10}\right) - b_{fl,8}\right] - \frac{b_{fl,9}}{2}\left[\left(\frac{p}{10}\right)^2 - {b_{fl,8}}^2\right]\right\} \quad (1)$$

$$h_{fv} = -100.R\left\{-b_{fv,1} + b_{fv,2}b_{fv,3} + \frac{b_{fv,4}}{2}\left[{b_{fv,3}}^2 + \left(\frac{T}{100}\right)^2\right] + \frac{b_{fv,5}}{3}\left[{b_{fv,3}}^3 + 2\left(\frac{T}{100}\right)^3\right] - b_{fv,2}\left(\frac{T}{100}\right) - b_{fv,4}\left(\frac{T}{100}\right)^2 - b_{fv,5}\left(\frac{T}{100}\right)^3 - b_{fv,6}\left[b_{fv,7} - \left(\frac{p}{10}\right)\right] + b_{fv,8}\left[-\frac{4\left(\frac{p}{10}\right)}{\left(\frac{T}{100}\right)^3} + \frac{4b_{fv,7}}{{b_{fv,3}}^3}\right] + b_{fv,9}\left[-\frac{12\left(\frac{p}{10}\right)}{\left(\frac{T}{100}\right)^{11}} + \frac{12b_{fv,7}}{{b_{fv,3}}^{11}}\right] + \frac{b_{fv,10}}{3}\left[-\frac{12\left(\frac{p}{10}\right)^3}{\left(\frac{T}{100}\right)^{11}} + \frac{12{b_{fv,7}}^3}{{b_{fv,3}}^{11}}\right]\right\} \quad (7)$$

where the coefficients of Equations (6) and (7) can be seen in **Table A.5**, respectively.

In addition, the effect of non-ideal solutions on ammonia-water causes enthalpy and entropy deviations from the ideal conditions. This deviation is known as excess enthalpy (Smith et al., 2018). The excess enthalpy and entropy modeling of ammonia-water can be carried out using numerical equations by B. Ziegler and C. Trepp (Ziegler & Trepp, 1984) in Equations (8) and (11).

$$h_E = -100.R.x.(1-x).\left\{\begin{array}{l}\left[-b_{E,1} - b_{E,2}\left(\frac{p}{10}\right) - \frac{2b_{E,3}}{\left(\frac{T}{100}\right)} - \frac{3\,b_{E,4}}{\left(\frac{T}{100}\right)^2}\right] \\ +(2x-1)\left[-b_{E,5} - b_{E,6}\left(\frac{p}{10}\right) - \frac{2b_{E,7}}{\left(\frac{T}{100}\right)} - \frac{3\,b_{E,8}}{\left(\frac{T}{100}\right)^2}\right] \\ +(2x-1)^2\left[-b_{E,9} - b_{E,10}\left(\frac{p}{10}\right) - \frac{2b_{E,11}}{\left(\frac{T}{100}\right)} - \frac{3b_{E,12}}{\left(\frac{T}{100}\right)^2}\right]\end{array}\right\} \tag{2}$$

which the coefficients of Equation (8) can be seen in **Table A.6**.

$$\begin{aligned} s_{fl} = -R\Bigg\{ & -b_{fl,1} + b_{fl,2} + \frac{b_{fl,3}}{2}\left(2\frac{T}{100}\right) + \frac{b_{fl,4}}{3}\left[3\left(\frac{T}{100}\right)^2\right] - \left[b_{fl,2}\ln\frac{\left(\frac{T}{100}\right)}{b_{fl,5}} + 1\right] - \left[b_{fl,3}\left(2\frac{T}{100}\right) - b_{fl,5}\right] \\ & - \frac{b_{fl,3}}{2}\left[3\left(\frac{T}{100}\right)^2 - {b_{fl,5}}^2\right] + \left[b_{fl,6} + 2b_{fl,7}\left(\frac{T}{100}\right)\right]\left[\left(\frac{p}{10}\right) - b_{fl,8}\right]\Bigg\} \end{aligned} \tag{3}$$

$$\begin{aligned} s_{fv} = -R\Bigg\{ & -b_{fv,1} + b_{fv,2} + b_{fv,3}\left(\frac{T}{100}\right)^2 - b_{fv,1}\left[1 + \ln\frac{\left(\frac{T}{100}\right)}{b_{fv,5}}\right] - b_{fv,3}\left[2\left(\frac{T}{100}\right) - b_{fv,5}\right] - \frac{b_{fv,4}}{2}\left[3\left(\frac{T}{100}\right)^2 - {b_{fv,5}}^2\right] \\ & + \ln\left(\frac{\left(\frac{p}{10}\right)}{b_{fv,6}}\right) + b_{fv,7}\left[-\frac{3\left(\frac{p}{10}\right)}{\left(\frac{T}{100}\right)^4} + \frac{3b_{fv,6}}{{b_{fv,5}}^4}\right] + b_{fv,8}\left[-\frac{11\left(\frac{p}{10}\right)}{\left(\frac{T}{100}\right)^{12}} + \frac{11b_{fv,6}}{{b_{fv,5}}^{12}}\right] \\ & + \frac{b_{fv,9}}{3}\left[-\frac{11\left(\frac{p}{10}\right)^3}{\left(\frac{T}{100}\right)^{12}} + \frac{11{b_{fv,6}}^3}{{b_{fv,3}}^{12}}\right]\Bigg\} \end{aligned} \tag{4}$$

where the coefficients of equations (9) and (10) can be seen in **Table A.7** respectively.

$$s_E = -R.x.(1-x).\left\{\begin{array}{l}\left[b_{E,1} + b_{E,2}\left(\frac{p}{10}\right) - \frac{b_{E,3}}{\left(\frac{T}{100}\right)^2} - \frac{2b_{E,4}}{\left(\frac{T}{100}\right)^3}\right] \\ +(2x-1)\left[b_{E,5} + b_{E,6}\left(\frac{p}{10}\right) - \frac{b_{E,7}}{\left(\frac{T}{100}\right)^2} - \frac{2b_{E,8}}{\left(\frac{T}{100}\right)^3}\right] \\ +(2x-1)^2\left[\frac{-b_{E,9}}{\left(\frac{T}{100}\right)^2} - \frac{2b_{E,10}}{\left(\frac{T}{100}\right)^3}\right]\end{array}\right\} \tag{5}$$

The coefficients of Equation (11) can be seen in **Table A.6**.

The basic modeling of enthalpy and entropy can use the specific heat coefficient parameters for each type of phase, the liquid phase equations can be seen in Equations (12) and (13) and the vapor phase equations can be seen in Equations (14) and (15) (Smith et al., 2018),

$$h_l^{id} = \int_{298.15}^{T} C_{p,l}\,dT \tag{6}$$

$$s_l^{id} = \int_{298.15}^{T} C_{p,l}\frac{dT}{T} - R\,ln\frac{p_T}{p_{298.15}} \tag{7}$$

$$h_v^{id} = h_l^{id} + h_{lv} + \int_{T_{lv}}^{T} C_{p,v}\,dT \tag{8}$$

$$s_v^{id} = s_l^{id} + \frac{h_{lv}}{T_{lv}} + \int_{T_{lv}}^{T} C_{p,v} \frac{dT}{T} - R\, ln \frac{p_T}{p_{298.15}} \quad (9)$$

by using the specific heat parameter values for pure water and [EMIM][DMP] in the liquid phase which is calculated by the empirical equation by J. Ren et al. (Ren et al., 2011), as shown in Equation (A.1) using the coefficients in **Table A.8**. Changing the fluid phase of water-[EMIM][DMP] involves latent heat that needs to be calculated using the Clausius/Clapeyron equation. This equation can only be used under low temperature and pressure (subcritical) (Smith et al., 2018).
In addition, the effect of the non-ideal solution on the water-[EMIM][DMP] causes enthalpy and entropy deviations of the mixture from its ideal condition. This deviation is known as excess enthalpy (Smith et al., 2018). The Redlich-Kister equation is one of the basic models of enthalpy and excess entropy that is often used (Ren et al., 2011), as seen in Equation (16). In the gas phase, generally, the mixing can be assumed to be ideal so that the excess enthalpy value can be neglected (Smith et al., 2018),

$$\frac{h^E}{x_1 x_2} = \sum_{i=1}^{4} b_i \, (2x_i - 1)^{i-1} \quad (16)$$

with empirical coefficients for water-[EMIM][DMP] as shown in **Table A.9**.

4.4. Optimization

The optimization process is carried out by determining the fixed parameters and variation parameters. Fixed parameters for each working fluid can be seen in **Error! Reference source not found.**.

Table 3: Fixed parameters of KCS 34.

Parameters	Water-[EMIM][DMP]		Ammonia-water	
	Value	Unit	Value	Unit
Fluida mass flow rate	5	kg/s	5	kg/s
Condenser pressure	0.1	bar	1.2	MPa

Optimization was done only by reviewing the thermodynamic aspect, namely varying the values of the cycle operating parameters. There are two operating parameters, namely turbine inlet pressure (TIP), and mass fraction of [EMIM][DMP] (x) whose values can be seen in **Table 4**. The upper limit of the independent variable is determined based on the evaporation temperature value which is the same as the brine inlet temperature value.

Table 4: Optimization parameters of KCS 34.

Parameters	Value	Lower limit	Higher limit	Interval
Turbine inlet pressure (TIP)	bar	1	7	1
Mass fraction of [EMIM][DMP] (x)	%	10	90	10

The optimization process on the ammonia-water fluid was carried out with the mass fraction of the ammonia mass fraction of 80—88%, turbine inlet pressure is around 30 bar, and the condenser pressure is equal to the saturated vapor pressure at the working fluid temperature at the temperature of the air as a cooling fluid added with *pinch point temperature* of 10°C which is supported by research conducted by Prananto et al. which used pressure of 11 bar (Prananto et al., 2018).

4.5. Economics Modelling

Economics modeling was carried out by calculating the estimated required capital costs of the two KCS 34 with ammonia-water and water-[EMIM][DMP] fluids. In addition, it was also determined the gross income obtained from the operation of the system so that the payback period can be calculated. AACE International (*American Association of Cost Engineering*) (Shabani & Yekta, 2006) classifies the feasibility study stage to calculate the cost of capital on a component basis. The component-based method commonly used is the Module Costing Method. The Module Costing Method uses the relationship between the capacity parameters of a component under operating conditions and costs under basic conditions, namely environmental conditions and uses a material that has been used massively, namely carbon steel. The basic equation used in this method uses component cost parameters in basic and operating conditions involving the component model used, material factors, and operating pressure factors. The two-parameter equations can be seen in Equations (17) and (18). Symbol Z is calculated based on the specifications of each component represented by one parameter, as can be seen in **Table B.1**. In addition to the main component costs, the calculation of the estimated cost of capital also involves other supporting factors grouped into indirect costs, as shown in
Table 5.

$$\log_{10}(C_{komp}^0) = K_1 + K_2 \log_{10}(Z) + K_3 (\log_{10}(Z))^2 \quad (17)$$

$$C_{komp} = C_{komp}^0 F_{BM,komp} = C_{komp}^0 (B_{1,komp} + B_{2,komp} F_{M,komp} F_{p,komp}) \quad (18)$$

Table 5: Indirect cost

Indirect cost components	Value (% total of main component capital cost)
Piping and installation	10
Control system and electricity	5
Construction	10
Engineer and supervisor services	5
Civil and structural works	30

The income calculated is gross income, which is the total income minus the cost of goods sold which is assumed to be the same as the operating and maintenance costs of the system (Gao & Chen, 2018). Gross income can be estimated using Equation (19),

$$Gross\ income\ per\ year = (CF.\dot{W}_{net}.OT.C_{listrik}) - C_{OM} \quad (19)$$

Based on International Renewable Energy Agency (IRENA) (IRENA, 2017), geothermal energy can provide a capacity factor value greater than other renewable energies, namely 85%. The payback time is calculated using Equation (20).

$$Payback\ Period = \frac{C_{2021}}{((CF.\dot{W}_{net}.OT.C_{listrik}) - C_{OM}).(1-i)} \quad (20)$$

5. VALIDATION AND RESULT

5.1. General

The validation process is necessary for modeling a system so that the modeling results can be accepted and accounted for. The validation process was conducted by comparing the results of the modeling with a credible reference. The validation process was carried out in the same range of conditions as the use of modeling. Thermodynamics modeling can be extrapolated if the existing validation reference data is very limited so that the analysis becomes more efficient and simple (Smith et al., 2018). In this study, two kinds of modeling validation were carried out, namely the validation of the thermodynamic properties of water-[EMIM][DMP] and the Kalina Cycle 34 modeling. After the validation was carried out and yielded valid results, the research continued with simulations.

Based on the simulations that have been carried out, the optimum point was obtained at the mass fraction [EMIM][DMP] of 30% and the turbine inlet pressure of 6.1 bar which results in thermal efficiency and a maximum net power of 8.81% and 343.23 kW, respectively. The T-s diagram of the operation at the optimum point can be seen in Figure 3.

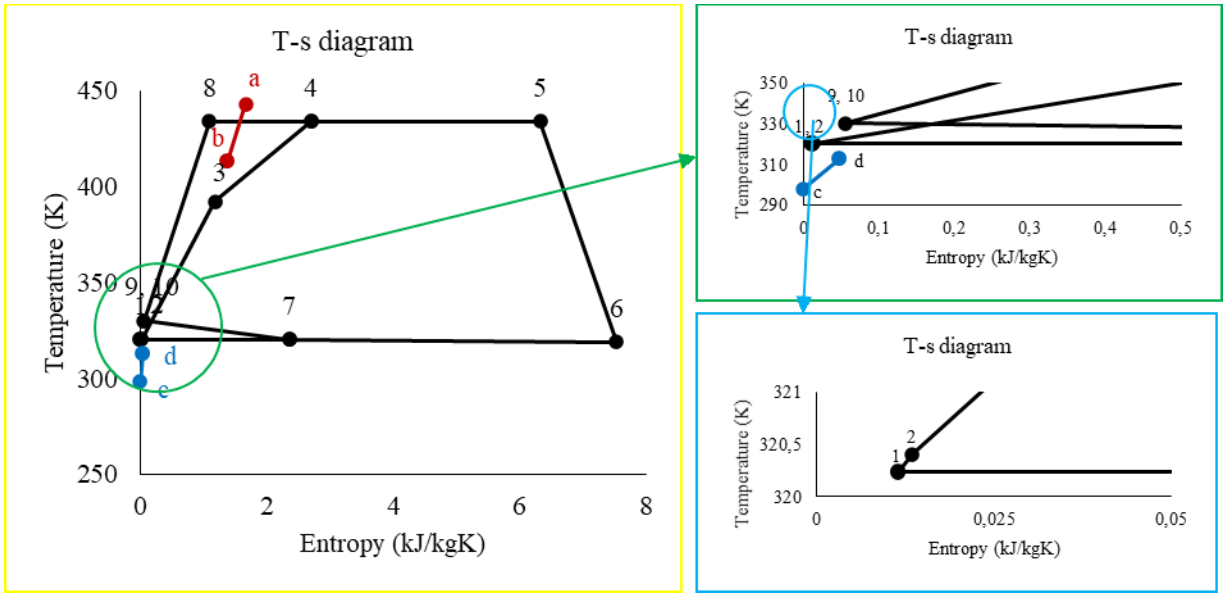

Figure 3: T-s diagram of KCS 34 water-[EMIM][DMP] at the optimum point.

5.2. Validation

The process of validating the thermodynamic properties of the mixed water-[EMIM][DMP] fluid was carried out on the numerical equations used in the Kalina Cycle 34 modeling from the cited references. The validated equations are the Antoine equation, NRTL, and Redlich-Kister for excess enthalpy, and specific heat. All of these equations were modeled numerically from the experimental process

conducted by J. Ren et al. (Ren et al., 2011) and J. Wang et al. (Wang et al., 2007). The experimental results are used as a reference as a validation reference for modeling and using these equations in MATLAB. In Table 6, it can be seen that the maximum relative error obtained is lower than 10% so it can be considered valid and accepted (Hoyos-Madrigal & Chejne-Janna, 2015). The highest relative error generated is about 6.21%. The maximum error in modeling is caused by the accumulation of errors from several equations used in calculating parameters such as the NRTL and Antoine equations. In addition, the maximum error is also caused by a small parameter value.

Table 6: The validation results of water-[EMIM][DMP] thermodynamic properties.

Equation	Maximum relative error (%)
Antoine	1.79
NRTL by J. Wang et al.	
Activity coefficients	3.10
Saturated vapor pressure	3.30
NRTL by J. Ren et al.	
Activity coefficients	6.21
Saturated vapor pressure	6.14
Redlich-Kister	0.98
Specific heat capacity	1.20

The process of validation of the Kalina Cycle 34 modeling is carried out by comparing the simulation results in MATLAB with the parameters in the reference at the same operating point. This modeling was only carried out on ammonia-water fluid because until this research is completed there has been no reference to simulate the water-[EMIM][DMP] fluid on the Kalina Cycle 34. The reference used is the Kalina Cycle 34 simulation conducted by X. Li et al. (Li et al., 2013). In **Table 7** it can be seen that the relative error obtained is lower than 10% so it can be considered valid and accepted (Hoyos-Madrigal & Chejne-Janna, 2015). The highest relative error occurs at the turbine exit temperature of 8.22%. The maximum error in modeling is caused by the accumulation of errors from several equations used in calculating parameters such as parameter iteration equations, NRTL, enthalpy, and entropy. In addition, the maximum error is caused by a small parameter value.

Table 7: The validation result of KCS 34 modeling.

Parameter	Unit	Xinguo Li, et al.	MATLAB simulation	
			Value	Error (%)
Heat source parameter				
Mass flow rate	kg/s	1	1	-
Evaporator inlet temperature	°C	110	110	-
Evaporator outlet temperature	°C	70.98	70.98	-
Ammonia-water parameter				
Mass fraction of ammonia		0.606	0.606	-
Evaporator inlet temperature	°C	65.98	65	1.49
Evaporator outlet temperature	°C	105	108.98	3.79
Separator outlet temperature	°C	105	108.98	3.79
Turbine outlet temperature	°C	71.2	77.05	8.22
Preheater outlet temperature	°C	45.1	45.1	-
Condenser inlet temperature	°C	66.08	69.96	5.87
Condenser outlet temperature	°C	35	35	-
Pump outlet temperature	°C	35.1	35.25	0.43
Evaporating pressure	MPa	1.55	1.55	-
Condensing pressure	MPa	0.69	0.69	-
Turbine outlet pressure	MPa	0.69	0.69	-
Mass flow rate	kg/s	0.24	0.24	-
Thermal cycle performance				
Heat at evaporator	kW	164.15	163.83	0.19
Heat at preheater	kW	40.87	38.39	6.07
Heat at condenser	kW	151.38	150.89	0.32
Turbine power	kW	13.04	13.05	0.08
Pump power	kW	0.27	0.27	0.00
Thermal efficiency	%	7.78	7.8	0.26

5.3. Thermodynamics Performance

The simulation results at the constant turbine inlet pressure (TIP) show the evaporating temperature (T_{ev}) increases with the increase in mass fraction of [EMIM][DMP] in the fluid. At a certain point, the temperature leads to a convergent of about 160°C as can be seen in

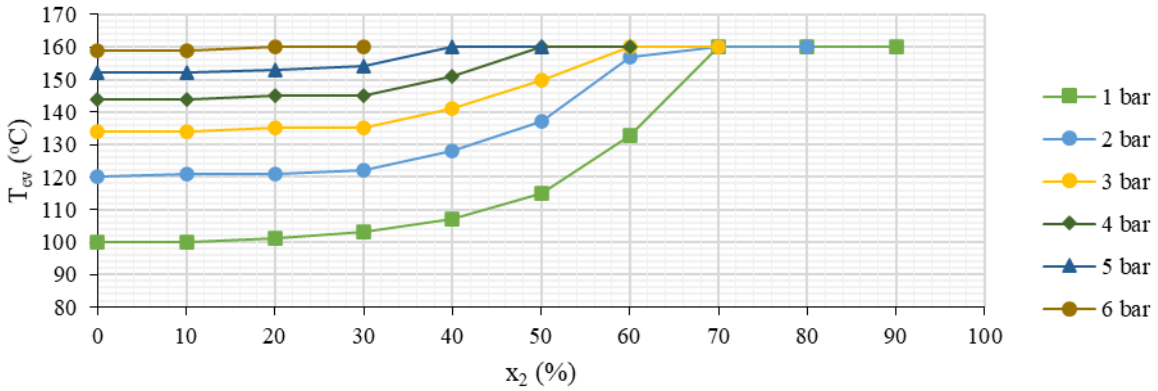

Figure 4 because the evaporation process is limited by the specifications on the evaporator component, namely the pinch point temperature of 10°C, so by using a heat source with a temperature of 170°C the maximum temperature of the fluid during the evaporation process is 160°C. The increase in evaporating temperature affects the enthalpy of the fluid when it exits the evaporator which is related to the electrical power generated in the turbine.

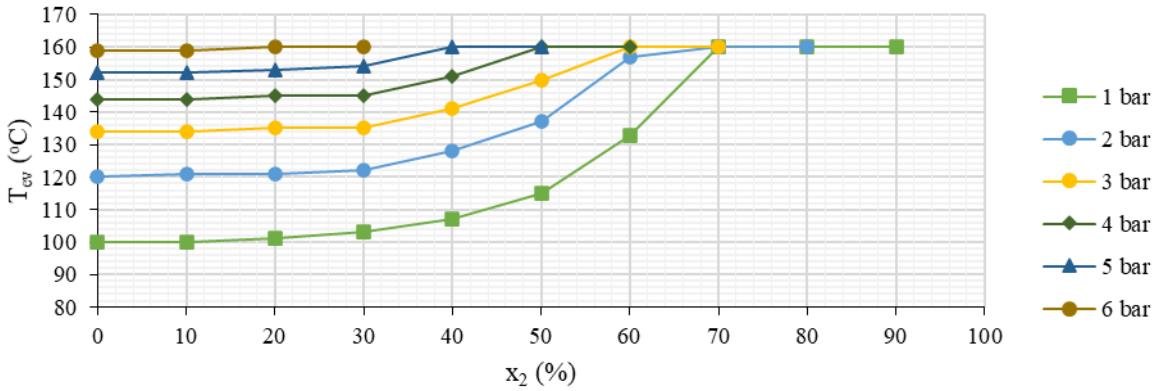

Figure 4: T_{ev} of KCS 34 of water-[EMIM][DMP] to x_2 at constant TIP.

Electrical power determines the cycle performance level. One of the performance comparison parameters for each power cycle through the products is net power. In the KCS 34 simulation using water-[EMIM][DMP] fluid at constant pressure, the net power parameter increases and decreases which are separated by one peak point, thus forming an open downward curve as can be seen in **Figure 5**. The turbine power produced by KCS 34 water-[EMIM][DMP] is determined by the mass flow rate of the fluid entering the turbine and also the enthalpy itself. The increase in both increases the turbine power and vice versa.

In the case of constant turbine inlet pressure, changes in mass fraction affect the values of these two parameters. The higher the mass fraction of [EMIM][DMP], the higher the boiling temperature of the water-[EMIM][DMP], as a result, the evaporation process produces lower vapor quality relative to the lower bubble temperature of the water-[EMIM][DMP] with the same heat source. On the other hand, an increase in the bubble temperature of the water-[EMIM][DMP] results in an increase in the enthalpy of the working fluid due to the higher the temperature, the higher the specific heat of water-[EMIM][DMP], as a result, the higher the fluid enthalpy. The relationship between the mass faction of [EMIM][DMP] with turbine inlet mass flow rate and enthalpy shows that mass fraction influences increasing or decreasing turbine power at constant turbine inlet pressure conditions so that the optimization process results in each operation under these conditions is a peak point on the constant pressure curve as shown in **Figure 5**.

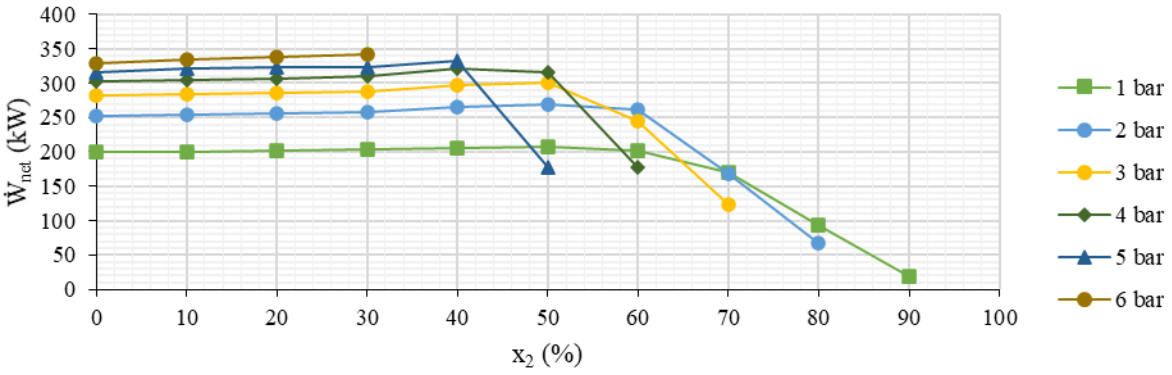

Figure 5: $\dot{W}_{net}$ of KCS 34 of water-[EMIM][DMP] to x_2 at constant TIP.

The resulting net power affects the thermal efficiency of KCS 34. In the use of the same heat source, the higher net power results in an increase in the thermal efficiency of KCS 34, so the effect of mass fraction of [EMIM][DMP] can affect the thermal efficiency of KCS 34 as can be seen in **Figure 6**. The high mass fraction condition undergoes an evaporation process at the maximum temperature limit of the evaporator due to the pinch point temperature difference (PPTD) specification on these components, resulting in very low quality of steam produced and very low mass flow rate entering the turbine. However, the mass flow rate entering the recuperator is higher when compared to the low mass fraction of [EMIM][DMP] operation making the heat transferred to the component larger with the limitations of the evaporator specifications, need for heat transferred from the brine is smaller. In other words, utilization of heat sources can be lower. Beside the decrease in the net power, there is also a decrease in the heat requirement of the evaporator, resulting in a certain thermal efficiency for each mass fraction of [EMIM][DMP].

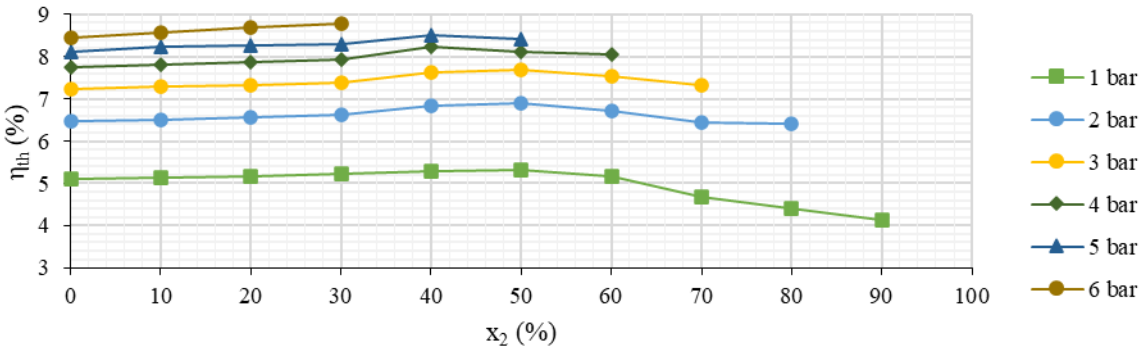

Figure 6: η_{th} of KCS 34 of water-[EMIM][DMP] to x_2 at constant TIP.

5.4. Economics Performance

The process of calculating the economic aspects of the Kalina Cycle 34 was carried out at each optimum point for water-[EMIM][DMP] and ammonia-water fluids. The calculated economic aspect parameters are the estimated capital cost, gross income, and the payback period as shown in Table 8.

Table 8: Economic calculation results of KCS 34.

Description (unit)	Qty	Value	Qty	Value
		KCS 34 Ammonia-water		KCS 34 Water-[EMIM][DMP]
A. Main component (pcs)				
Pump	1	$ 32,992.78	1	$ 17,144.56
Preheater	1	$ 159,559.37	1	$ 150,224.95
Evaporator	1	$ 175,508.74	1	$ 227,999.84
Steam turbine	1	$ 959,348.43	1	$ 965,969.37
Expansion valve	1	$ 26.90	1	$ 13.45
Condenser	1	$ 330,901.77	1	$ 352,789.67
Total of the main component		$ 1,658,337.99		$ 1,714,141.84
B. Working fluids (kg)				

Working fluid	4.3	$	1.51	1.5	$ 10,800.00
C. Auxiliary component (% main component value)					
Piping and installation	10	$	165,833.80	10	$ 171,414.18
Control system and electricity	5	$	82,916.90	5	$ 85,707.09
Construction	10	$	165,833.80	10	$ 171,414.18
Engineer and supervisor services	5	$	82,916.90	5	$ 85,707.09
Civil and structural works	30	$	497,501.40	30	$ 514,242.55
Total of auxiliary components		$	995,002.79		$ 1,028,485.10
Total capital cost		$	2,653,342.29		$ 2,753,426.94
Revenue		$	346,542.63		$ 364,487.20
Operational costs					
Operation and maintenance (% capital costs)	1.65	$	43,780.15	1.65	$ 45,431.54
Total gross income		$	302,762.49		$ 319,055.66
Payback period (year)			9.1		9

5.5. Comparison to the results of KCS 34 with Ammonia-water

The optimum point of KCS 34 for ammonia-water fluid is sought in the optimization range of parameters that have been discussed in Section 4.6. At the optimum point, the operating points of ammonia-water and water-[EMIM][DMP] fluids are obtained using thermodynamic assumptions and heat sources, as shown in Table 9.

Table 9: Optimum point of KCS 34.

Parameter	Unit	Water-[EMIM][DMP]	Amonia-water
Mass fraction of [EMIM][DMP] or ammonia	wt%	30	86
Mass flow rate	kg/s	5	5
Condensing pressure	bar	0.1	12
Pump inlet temperature	°C	47.2	37.2
Turbine inlet pressure	bar	6	31

Table 9 shows that the operating pressure of the ammonia-water fluid is much higher than the operating pressure of the water-[EMIM][DMP] fluid because ammonia has a much lower boiling temperature than [EMIM][DMP], so high pressure is needed to adapt to environmental conditions and the heat source used. The operation of KCS 34 at the optimum point produces parameters that can be seen in **Table 10**.

Table 10: Performance parameters comparison of KCS 34.

Parameter	Unit	Water-[EMIM][DMP]	Ammonia-water
Pump power	kW	3.34	15.84
Turbine power	kW	346.57	342.17
Thermal efficiency	%	8.81	8.37

Table 10 shows that the power required by the pump to increase the fluid pressure of water-[EMIM][DMP] is lower than that of ammonia-water, which is about 78.9% lower because of the optimum operating pressure point differs greatly between the two. Furthermore, the turbine power produced by the water-[EMIM][DMP] fluid is slightly higher than the ammonia-water, which is about 1.29%, so with the same heat source, the thermal efficiency produced by the water-[EMIM][DMP] fluid is approximately 5.18% higher than that of the ammonia-water fluid. Although the turbine power increase is only 1.29%, the pump power consumption which is much lower than that of ammonia-water can provide a large net power difference of 5.18%, so the difference in thermal efficiency is greater.

From an economic point of view, **Table 8** shows the estimated value of capital costs for KCS 34 with water-[EMIM][DMP] fluid which is higher than ammonia-water which is about 3.77% more expensive because the heat exchanger uses relatively smaller PPTD parameters and has a larger turbine power capacity. In addition, the cost of procuring working fluid [EMIM][DMP] is more expensive than ammonia-water. The gross income which can be obtained by KCS 34 with water-[EMIM][DMP] fluid is higher than ammonia-water by about 5.38% because the net power generated by KCS 34 with fluid is higher than ammonia-water. The payback period for KCS 34 using water-[EMIM][DMP] fluid is slightly faster than ammonia-water, which is about one month. Both have a payback period of fewer than thirty years so that both cycles can each provide profit in the remaining operating period from the sales of electricity generated by the system.

6. CONCLUSIONS

From the results of the thermodynamic and economic analysis of KCS 34, several conclusions can be drawn as follow:

1. The modeling of the thermodynamic properties of water-[EMIM][DMP] and the Kalina Cycle 34 with MATLAB R2020b software resulted in a maximum error of 6.21% and 8.22%, respectively.

2. Water-[EMIM][DMP] fluid can be used in the Kalina Cycle 34. Based on the optimization results, the Kalina Cycle 34 has maximum thermal efficiency and a net power of 8.81% and 343.23 kW, respectively. This is 5.18% higher than the thermal efficiency and maximum net power of ammonia-water fluid at the same heat source which is 8.37% and 326.33 kW with non-toxic chemical properties which is more environmentally friendly than ammonia-water fluid.
3. From the results of the estimated cost of capital and the required payback period in the utilization of water-[EMIM][DMP] fluid in the Kalina Cycle 34, the cycle requires an estimated capital cost of $2,753,426.94. This is 3.77% higher than the estimated required for ammonia-water fluid of $2,653,342.29 and the return on investment of the Kalina Cycle System 34 with water-[EMIM][DMP] requires 9 years from the beginning of operation of the system. In other words, this is one month faster than ammonia-water which is 9 years and 1 month.
4. The results of calculating the estimated gross income that can be obtained from the operation of the Kalina Cycle System 34 using water-[EMIM][DMP] fluid is about $319,055.66/year or 5.38% higher than the gross income that can be obtained when using ammonia-water which is $302,762.49/year

REFERENCES

Ahmad, M., & Karimi, M. N.: Thermodynamics Analysis of Kalina Cycle. International Journal of Science and Research (ISSR), 5(3), 2244–2249. (2016).

Asian Development Bank.: Indicative Lending Rates for Loans under the LIBOR-Based Loan Facility. Indicative Lending Rates for Loans under the LIBOR-Based Loan Facility. (2021).

Bacharach.: Bacharach Gas Detection & Analysis Expert:Ammonia (R-717) Gas Detection,. Bacharach Gas Detection & Analysis Expert:Ammonia (R-717) Gas Detection. (2020). https://www.mybacharach.com/ammonia-nh3-gas-detection/

Badan Geologi.: Klasifikasi Temperatur Reservoir dan Pemanfaatan Sumber Daya Panas Bumi, Kementerian ESDM. Klasifikasi Temperatur Reservoir Dan Pemanfaatan Sumber Daya Panas Bumi, Kementerian ESDM. (2018). http://psdg.bgl.esdm.go.id/index.php?option=com_content&view=article&id=1239&Itemid=610

D. Mendrinos et al.: Geothermal Binary Plants: Water or Air Cooled. Geothermal Binary Plants: Water or Air Cooled. (2020). http://energybc.ca/cache/hightempgeo/www.lowbin.eu/public/CRES-GeothermalBinaryPlants-Water or Air Cooled.pdf

DiPippo, R.: Geothermal Power Plants. In Geothermal Power Plants. (2005). https://doi.org/10.1016/B978-1-85617-474-9.X5029-8

Energia News.: PGE Selesaikan Turn Around PLTP Kamojang Lebih Cepat, Pertamina Geothermal Energy. PGE Selesaikan Turn Around PLTP Kamojang Lebih Cepat, Pertamina Geothermal Energy. (2021). https://www.pertamina.com/id/news-room/energia-news/pge-selesaikan-turn-around-pltp-kamojang-lebih-cepat

Franco, A., & Villani, M.: Optimal Design of Binary Cycle Power Plants For Water-Dominated, Medium-Temperature Geothermal Fields. Geothermics, 38, (2009) 379–391.

Gao, H., & Chen, F.: Thermo-Economic Analysis of a Bottoming Kalina Cycle for Internal Combustion Engine Exhaust Heat Recovery. Energies, 11, (2018) 3044–3063.

Hoyos-Madrigal, B. A., & Chejne-Janna, F. (2015). Comparison of Molecular Models of Carbon Monoxide for Calculation of Vapor-Liquid Equilibrium. Revista Facultad de Ingenieria, 1(75), 143–154.

Indiamart.: Parth Valves and Hoses LLP, Mild Steel Globe Valve, Indiamart. Parth Valves and Hoses LLP, Mild Steel Globe Valve. (2020). https://www.indiamart.com/proddetail/mild-steel-globe-valves-1165354688.html

IRENA.: Renewable Energy Prospects: Indonesia, a Remap analysis, International Renewable Energy Agency (IRENA). Renewable Energy Prospects: Indonesia, a Remap Analysis, International Renewable Energy Agency (IRENA). (2017). https://www.irena.org/-/media/Files/IRENA/Agency/Publication/2017/Mar/IRENA_REmap_Indonesia_report_2017.pdf

Kalina, A., Kaiina, M., Dickson, J., & Moore, S.: Evaluation and comparisons of currently available binary cycle geothermal power systems. Transactions - Geothermal Resources Council, 38, (2014) 777–788.

Khamooshi, M., Parham, K., & Atikol, U.: Overview of ionic liquids used as working fluids in absorption cycles. Advances in Mechanical Engineering. (2013). https://doi.org/10.1155/2013/620592

Kontan.co.id.: Perpres EBT sebut harga listrik dari IPP untuk PLTP capai US$ 14,50 sen per kWh. Perpres EBT Sebut Harga Listrik Dari IPP Untuk PLTP Capai US$ 14,50 Sen per KWh. (2020). https://industri.kontan.co.id/news/perpres-ebt-sebut-harga-listrik-dari-ipp-untuk-pltp-capai-us-1450-sen-per-kwh.

Frick, S., Saadat, A., Surana, T., Siahaan, E. E., Kupfermann, G. A., Erbas, K., Huenges, E., & Gani, M. A.: Geothermal Binary Power Plant for Lahendong , Indonesia : A German-Indonesian Collaboration Project. World Geothermal Congress 2015, (2015).

Kumara, C., Bandara, J., Abeyweera, R., & Senanayake, N. S. Minimizing Energy Loss by Optimizing Pipe Diameter and Insulation Thickness in Steam Distribution Pipelines Minimizing Energy Loss by Optimizing Pipe Diameter and Insulation Thickness in Steam Distribution Pipelines. (2015).

Li, X., Zhang, Q., & Li, X.: A Kalina cycle with ejector. Energy, 54, (2013) 212–219. https://doi.org/10.1016/j.energy.2013.03.040

Maxwell, C.: Cost Indices. (2020). https://www.toweringskills.com/financial-analysis/cost-indices/.

Moran, M. J., Saphiro, H. N., Boettner, D. D., & Bailey, M. B. Fundamental of Engineering Thermodynamics. In Wiley: Ed 8. (2014).

Novotny, V., & Kolovratnik, M.: Absorption Power Cycles for Low-Temperature Heat Sources Using Aqueous Salt Solutions as Working Fluids. International Journal of Energy Research. (2016).

Pátek, J., & Klomfar, J.: Simple functions for fast calculations of selected thermodynamic properties of the ammonia-water system. International Journal of Refrigeration, 18(4), (1995) 228–234. https://doi.org/10.1016/0140-7007(95)00006-W

Rencana Umum Energi Nasional.: Rencana Umum Energi Nasional (2017). https://www.esdm.go.id/assets/media/content/contentrencana-umum-energi-nasional-ruen.pdf

Pranantо, L. A., Zaini, I. N., Mahendranata, B. I., Juangsa, F. B., Aziz, M., & Soelaiman, T. A. F.: Use of the Kalina Cycle as a Bottoming Cycle in a Geothermal Power Plant: Case Study of the Wayang Windu Geothermal Power Plant. Applied Thermal Engineering, 132, (2018) 686–696.

Putera, A. D. P., Hidayah, A. N., & Subiantoro, A.: Thermo-economic analysis of a geothermal binary power plant in Indonesia—a pre-feasibility case study of the Wayang Windu site. Energies, 12(22). (2019). https://doi.org/10.3390/en12224269

Ranjan, R. K., Haldkar, V., Sharma, A. K., & V.K. Bajpai.: An Energy Analysis of Condenser. International Journal of Thermal Technologies, 3(4), (2013) 120–125.

Ren, J., Zhao, Z., & Zhang, X.: Vapor pressures, excess enthalpies, and specific heat capacities of the binary working pairs containing the ionic liquid 1-ethyl-3-methylimidazolium dimethylphosphate. J. Chem. Thermodynamics, 43, (2011) 576–583.

Shabani, M. R., & Yekta, R. B.: Suitable Method for Capital Cost Estimation in Chemical Processes Industries. Cost Engineering, 48, (2006) 22–25.

Smith, J. M., Van Ness, H. C., Abbott, M. M., & Swihart, M. T.: Introduction to chemical engineering thermodynamics (8th ed.). McGraw-Hill Education. (2018). https://doi.org/10.1021/ed027p584.3

Wang, J., Li, C., Wang, Z., Li, Z., & Jiang, Y.: Vapor pressure measurement for water , methanol , ethanol , and their binary mixtures in the presence of an ionic liquid 1-ethyl-3-methylimidazolium dimethylphosphate. 255, (2007) 186–192. https://doi.org/10.1016/j.fluid.2007.04.010.

Zhang, X., He, M., & Zhang, Y.: A Review of Research on The Kalina Cycle. Renewable and Sustainable Energy Reviews, 16, (2012) 5309–5318

Zhang, X., & Hu, D.: Performance simulation of the absorption chiller using water and ionic liquid 1-ethyl-3-methylimidazolium dimethylphosphate as the working pair. Applied Thermal Engineering, 31(16), (2011) 3316–3321. https://doi.org/10.1016/j.applthermaleng.2011.06.011

Ziegler, B., & Trepp, C.: Equation of state for ammonia-water mixtures. 7(2), (1984) 101–106

APPENDIX

APPENDIX A

Table A.1: Bubble and dew temperature equation coefficients (Pátek & Klomfar, 1995).

i	Bubble temp. eq. coefficient			Dew temp. eq. coefficient		
	m_i	n_i	b_i	m_i	n_i	b_i
1	0	0	3.22302	0	0	3.24004
2	0	1	-3.84206 x 10^{-1}	0	1	-3.95920 x 10^{-1}
3	0	2	4.60965 x 10^{-2}	0	2	4.35624 x 10^{-2}
4	0	3	-3.78945 x 10^{-3}	0	3	-2.18943 x 10^{-3}
5	0	4	1.35610 x 10^{-4}	1	0	-1.43526
6	1	0	4.87755 x 10^{-1}	1	1	1.05256
7	1	1	-1.20108 x 10^{-1}	1	2	-7.19281 x 10^{-2}
8	1	2	1.06154 x 10^{-2}	2	0	1.22362 x 10^{1}
9	2	3	-5.33589 x 10^{-4}	2	1	-2.24368
10	4	0	7.85041	3	0	-2.01780 x 10^{1}
11	5	0	-1.15941 x 10^{1}	3	1	1.10834
12	5	1	-5.23150 x 10^{-2}	4	0	1.45399 x 10^{1}
13	6	0	4.89596	4	2	6.44312 x 10^{-1}
14	13	1	4.21059 x 10^{-2}	5	0	-2.21246
15	0	0	0	5	2	-7.56266 x 10^{-1}
16	0	0	0	6	0	-1.35529
17	0	0	0	7	2	1.83541 x 10^{-1}

Table A.2: Antoine equation coefficient for water (Ren et al., 2011).

Coefficient	Value
b_1	1.628837 x 10^{1}
b_2	-3.8164 x 10^{3}
b_3	-4.613 x 10^{1}

Table A.3: Constant and coefficient of NRTL by J. Ren et al. (Ren et al., 2011).

i	a_i	b_i	c_i	α
1	-4.04950175 x 10^{5}	2.183902 x 10^{3}	-2.81	6.004 x 10^{-1}
2	-7.58911 x 10^{3}	1.0215 x 10^{1}	-3.56 x 10^{-2}	

Table A.4: Constant and coefficient of NRTL by J. Wang et al (Wang et al., 2007).

b_{12}	b_{21}	α
1.256 x 10^{1}	-8,824.4	3.594 x 10^{-1}

Table A.5: Enthalpy equation coefficient of pure ammonia and water (Ziegler & Trepp, 1984).

i	$b_{fl,i}$		$b_{fv,i}$	
	ammonia	water	ammonia	water
1	4.878573	2.1821141 x 10^{1}	2.6468879 x 10^{1}	6.0965058 x 10^{1}
2	1.634519 x 10^{1}	1.214557 x 10^{1}	3.673647	4.019170
3	3.2252	5.0705	3.2252	5.0705
4	-6.508119	-1.898065	9.989629 x 10^{-2}	-5.175550 x 10^{-2}
5	1.448937	2.911966 x 10^{-2}	3.617622 x 10^{-2}	1.951939 x 10^{-2}
6	3.752836 x 10^{-3}	8.389246 x 10^{-4}	-1.049377 x 10^{-2}	2.136131 x 10^{-2}
7	3.971423 x 10^{-2}	2.748796 x 10^{-2}	2	3
8	2	3	-8.288224	-3.169291 x 10^{1}
9	-1.790557 x 10^{-5}	-1.016665 x 10^{-5}	-6.647257 x 10^{2}	-4.634611 x 10^{4}
10	0	0	-3.045352 x 10^{3}	0

Table A.6: Excess enthalpy and entropy equation coefficient of ammonia-water (Ziegler & Trepp, 1984).

i	Enthalpy coefficient ($b_{E,i}$)	Entropy coefficient ($b_{E,i}$)
1	-4.626129 x 10^{1}	7.292369
2	2.060225 x 10^{-2}	-1.032613 x 10^{-2}
3	8.074824 x 10^{1}	8.074824 x 10^{1}
4	-8.461214 x 10^{1}	-8.461214 x 10^{1}
5	2.452882 x 10^{1}	-1.475383
6	9.598767 x 10^{-3}	-5.038107 x 10^{-3}
7	-9.640398 x 10^{1}	-9.640398 x 10^{1}
8	1.226973 x 10^{2}	1.226973 x 10^{2}
9	-7.582637	5.487018 x 10^{1}
10	6.012445 x 10^{-4}	-7.667596 x 10^{1}
11	5.487018 x 10^{1}	0
12	-7.667596 x 10^{1}	0

Table A.7: Entropy equation coefficient of pure ammonia and water (Ziegler & Trepp, 1984).

i	$b_{fl,i}$		$b_{fv,i}$	
	ammonia	water	ammonia	water
1	1.644773	5.33498	8.339026	1.3453430 x 10^{1}
2	1.634519 x 10^{1}	1.214557 x 10^{1}	3.673647	4.019170
3	-6.508119	-1.898065	9.989629 x 10^{-2}	-5.175550 x 10^{-2}
4	1.448937	2.911966 x 10^{-2}	3.617622 x 10^{-2}	1.951939 x 10^{-2}
5	3.2252	5.0705	3.2252	5.0705
6	-1.308905 x 10^{-2}	-4.452025 x 10^{-3}	2	3
7	3.752836 x 10^{-3}	8.389246 x 10^{-4}	-8.288224	-3.169291 x 10^{1}
8	2	3	-6.647257 x 10^{2}	-4.634611 x 10^{4}
9	0	0	-3.045352 x 10^{3}	0

The specific heat of pure water and [EMIM][DMP] in the liquid phase were calculated by empirical equations by J. Ren et al. (Ren et al., 2011) as shown in equation (A.1) using the coefficients in **Table A.12**.

$$c_{p,l} = \sum_{i=0}^{4} a_i x_2 + \sum_{i=0}^{4} b_i x_2 T \qquad \text{(A.1)}$$

where a_i and b_i are coefficient of the numerical equation as shown in **Table A.12**, while x_2 is mol fraction of [EMIM][DMP].

Table A.8: $C_{p,l}$ equation coefficient of water-[EMIM][DMP] (Ren et al., 2011).

Coeff.	i				
	0	1	2	3	4
a_i	-8.430997 x 10^{-1}	-2.05718268	1.38853919 x 10^{1}	3.13818543 x 10^{1}	-2.66425299 x 10^{1}
b_i	1.47825 x 10^{-2}	2.63706 x 10^{-2}	5.32389 x 10^{-2}	-2.078705 x 10^{-1}	1.275218 x 10^{-1}

Table A.9: Redlich-Kister equation coefficient of water-[EMIM][DMP] (Ren et al., 2011).

Fluids	b_1	b_2	b_3	b_4
water(1)-[EMIM][DMP](2)	-2.337900 x 10^{4}	-1.099960 x 10^{4}	-7.9099 x 10^{3}	-9.01657 x 10^{3}

APPENDIX B

The calculation of the capacity parameter (Z) and the values of the coefficients and other constants are unique to the components and are used in calculating the estimated capital cost.

Table B.1: Z parameter based on component (Shabani & Yekta, 2006).

Component	Z	Unit
Heat exchanger	Surface area	m^2
Pump	Power	kW
Turbine	Power	kW
Separator	Volume	m^3

The heat exchanger area can be determined or calculated for each type using the Log mean Temperature Difference (LMTD) equation. The value of U can be estimated based on the type of heat exchanger components, such as the evaporator, recuperator, and condenser which have a U value, namely 1100 W/m^2.^{o}C, 700 W/m^2.^{o}C, and 500 W/m^2.^{o}C respectively. The Z value of the separator is the volume of the separator. According to DiPippo (DiPippo, 2005), the size of the separator can be approximated using the diameter parameter of the separator inlet as shown in **Figure B.1**.

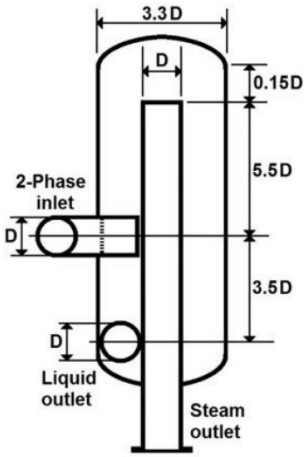

Figure B.1: Separator dimension (DiPippo, 2005).

The Z value of the pump is the power required by the pump to increase the pressure of a fluid, while the turbine is the power generated by the turbine. The parameters for calculating the estimated basic capital cost, the operating pressure factor on the components, and the estimated actual capital cost can be seen in **Tables B.3**, **B.4**, and **B.5**, respectively.

Table B.2: Basic capital cost parameter for each component (C_{kom}^0) (Shabani & Yekta, 2006).

Component	K_i
Heat exchanger	shell and tube type for $10 < A(m^2) < 1000$: $K_1 = 4.3247$, $K_2 = -0.303$, $K_3 = 0.1634$ Air cooled type for $10 < A(m^2) < 1000$: $K_1 = 4.0336$, $K_2 = 0.2341$, $K_3 = 0.0497$
Pompa	Centrifugal type for $1 < \dot{W}_{po}(kW) < 300$: $K_1 = 3.3892$, $K_2 = 0.0536$, $K_3 = 0.1538$
Separator	Vertical type for $0,3 < V(m^3) < 520$: $K_1 = 3.497$, $K_2 = 0.449$, $K_3 = 0.107$
Turbine	Axial type for $100 < \dot{W}_T(kW) < 4000$: $K_1 = 2.7051$, $K_2 = 1.4398$, $K_3 = -0.1776$

Table B.3: Pressure factor parameter ($F_{p,komp}$) (Shabani & Yekta, 2006).

Component	$F_{p,komp}$	C_i
Heat exchanger	$\log_{10} F_{p,komp} = C_{1,komp} + C_{2,komp} \log_{10}(p_{komp}) + C_{3,komp}(\log_{10}(p_{komp}))^2$	Shell and tube type for $5 < p(bar) < 40$: $C_1 = 0.03881$, $C_2 = 0.11272$, $C_3 = 0.08183$ Air cooled type for $10 < p(bar) < 100$: $C_1 = -0.125$, $C_2 = 0.15361$, $C_3 = -0.02861$
Pump		Centrifugal type for $10 < p(bar) < 100$: $C_1 = -0.3935$, $C_2 = 0.3957$, $C_3 = -0.00226$
Separator	$F_{p,sep} = max\left\{\frac{\frac{(p_{sep}+1)D_{sep}}{2[850-0,6(p_{sep}+1)]}+0,00315}{0,0063}, 1\right\}$	-

Table B.4: Actual capital cost for each component (C_{komp}) (Shabani & Yekta, 2006).

Component	$F_{BM,komp}$	$F_{M,komp}$	B_i	Actual capital cost
Heat exchanger	-	For carbon steel: $F_{M,komp}$ = 1	Shell and tube type: B_1 = 1.63, B_2 = 1.66 Shell and tube type: B_1 = 0.96, B_2 = 1.21	$C_{komp} = C^0_{komp}(B_{1,komp} + B_{2,komp}F_{M,komp}F_{p,komp})$
Pump			Centrifugal type: B_1 = 1.89, B_2 = 1.35	
Separator			Vertical type: B_1 = 2.25, B_2 = 1.82	
Turbine	3.5	-	-	$C_{komp} = C^0_{komp}F_{BM,komp}$

The actual capital costs for expansion valves were obtained from the component catalogs available at the component manufacturing company because there was no calculation in the module costing method for the component in question. Based on the LLP Parth Valves and Hoses manufacturing catalog, the latest 2021 prices for expansion valves of globe valve type with specifications meeting the water-[EMIM][DMP] operating point are around $13.45/unit, while in the Millennium Industrial Valves manufacturing catalog, the price of a valve with specifications meeting the ammonia-water operating point is around $26,90/unit (Indiamart, 2020).

The supporting cost components used in economic modeling are as follows:

- Operation and maintenance costs are estimated at 1.65% of the total capital cost (Gao & Chen, 2018).
- Bank loan interest rates are obtained from the Asian Development Bank loan interest data which refers to the London Interbank Offered Rate (LIBOR), the loan interest is LIBOR plus 0.5 percent per year. The highest LIBOR value for the past 5 years (2016-2020 (Asian Development Bank, 2021).
- The price of electricity used is the selling price of PLTP electricity based on the electricity price sold by the Independent Power Producer (IPP) to PLN from the draft Presidential Regulation on the Purchase of Renewable Energy Electricity by PT Perusahaan Listrik Negara, amounting to $14.50 /kWh (Kontan.co.id, 2020).
- Chemical Engineering Plant Cost Index (CEPCI) factors in 2001 and 2021 are 395 and 665.9, respectively (Maxwell, 2020).

NOMENCLATURE

Symbol	Description	Unit	Symbol	Description	Unit
A	Surface are	m^2	U	Overall heat transfer coefficient	$W/m^2.^oC$
b	Coefficient of an empirical equation	-	$\mathcal{V}$	Gas mol	kmol
C	Cost	USD	$\dot{W}$	Work	kW
CF	Capacity factor	-	x	Liquid mass fraction	kg/kg
Cp	Specific heat	kJ/kg.K	y	Vapor mass fraction	kg/kg
g	Earth's gravitational acceleration	m/s^2	**subscript**		
h	Specific enthalpy	kJ/kg	*1, 2, 3, …**	Empirical coefficient 1, 2, 3, …	
I	CEPCI factor	-	*1, 2, 3, …**	State 1, 2, 3, …	
i	Interest	%	*bbl*	Bubble	
$\dot{m}$	Mass flow rate	kg/s	*dew*	Dew	
OT	Operating time	h	*E*	Excess	
p	Pressure	bar	**superscript**		
ρ	Density	kg/m^3	*id*	Ideal gas	
$\dot{Q}$	Heat rate	kW	*l*	Liquid	
R	Ideal gas constant	kJ/kmol.K	*v*	Vapor	
s	Specific entropy	kJ/kg.K	*sat*	Saturated	
T	Temperature	^oC	*total*	Overall fluid	